ELM (Extreme Learning Machine) Based Correlated Interference Canceller for Small Aperture Array Antenna

Junseok LIM[1], *Heesuk PANG*[1], *Wooyoung HONG*[2]

[1]Dept. of Electronics Engineering, Sejong University, Seoul, Korea 143-747
[2]Dept. of Military System Engineering, Sejong University, Seoul, Korea 143-747

jslim@sejong.ac.kr, hspang@sejong.ac.kr, wyhong@sejong.ac.kr

Abstract. *The multipath effect creates a highly correlated interference; subsequently, small aperture array antennas equipped in mobile devices are required to effectively cancel this coherent interference. Spatial smoothing MMSE is a typical coherent interference cancellation algorithm; however, this method further reduces the small aperture size as well as the number of coherent interferences to cancel out. This paper proposes a new method to reject coherent interferences without a reduction in the antenna aperture size. We show the superiority of the proposed algorithm through a comparison of cancellation performance with existing adaptive beamforming algorithms.*

Keywords

Coherent interference cancellation, small aperture array antenna, ELM, MMSE, spatial smoothing.

1. Introduction

Mobile communication technology has developed extensively due to its popularity [1]-[4]. This popularity has increased the usage of personal communication devises that require a small aperture antenna (array antenna with small numbers of elements)[5],[6]. Space-time coding (a successful mobile communication technology) provides multiple-input multiple-output (MIMO) systems to increase channel capacity and spectral efficiency without additional bandwidth and power consumption [7],[8]. There is significant interest in array antennas that represent a promising scheme to improve the Signal to Interference Ratio (SIR) through the cancellation of interference signals in the received signal. Schemes to combined MIMO-smart antenna systems have been proposed. An overview of this technique is presented in [9]. In [10], it is shown that the scheme of MIMO wireless systems that incorporate a beamforming method before a space-time decoder can effectively mitigate CCI and preserve the space-time structure. [10] and [11] proposed an adaptive antenna array method to suppress the CCI in the trellis STC OFDM system. In addition, it has been shown that beamforming technology incorporated into the IEEE802.11ac standard can improve system performance, where the IEEE 802.11ac is a newly released WLAN standard [12], [13].

In general mobile communication environments, the received signal frequently develops from multipath environments. In such an environment, one component in the received signal becomes a scaled and delayed replica of the other; subsequently, multipath propagation creates a coherent interference [14], [15]. Therefore, the correlation between the two signals significantly increases if one is coherent to the other.

Many methods have been developed to cancel interference signals in received signals [16]. Most of the developed methods assume an uncorrelated interference; in addition, the beamforming output SIR severely deteriorates if these methods are applied to a received signal with a coherent interference. Evans et al. proposed a spatial smoothing algorithm (a representative method) to cancel the coherent interferences [17]; in addition, Kailath et al. analyzed the theoretical performance of the spatial smoothing algorithm [18].

The spatial smoothing method subdivides the whole array into overlapping subarrays that reduce the effective array elements (i.e. reducing the aperture size). An array antenna can cancel out up to N-1 interference signals, where N is the number of elements in the array. Spatial smoothing reduces the number of interferences to be canceled in the array antenna. This disadvantage becomes a serious problem in a small aperture array; however, it is minimal in a large aperture array.

Lo et al. produced unique research results in nonlinear beamforming based on linear beamforming [19]. The expected merits of the nonlinear beamforming are:

1. It is effective to estimate signals in different types of noise backgrounds, such as Gaussian, non-Gaussian, or colored noise.
2. It is robust to resolve multiple coherent signals.
3. It is capable of resolving signals separated by less than an antenna beamwidth.
4. It has very low sidelobes.

Item 3 of the summaries indicates that the nonlinear beamforming resolves multiple coherent signals by creating proper beams for every coherent signal, respectively. These results were for a fixed beamformer (not an adaptive beamformer) and there were no results for the interference cancellation [19]; however, it did indicate how to reject coherent interference signals. Recently, support vector machine (SVM) based nonlinear beamforming algorithms have been studied with results that indicate the interference rejection in the steering mismatch [20]-[23].

This paper proposes a nonlinear beamformer to cancel coherent interference signals using an Extreme Learning Machine (ELM). ELM is a newly developed single-hidden-layer feed forward network (SLFN). ELM applies random generated nodes in the hidden layer that may be independent of the training data [24]. The hidden layer of single layer network need not be tuned; consequently, it is popular for its fast training speed [24]-[26]. ELM also uses various nonlinear activation functions. These features show that ELM can be a nonlinear beamformer that can be trained as a linear beamformer. In addition, ELM can be applied to various types of beamformers because ELM can be implemented for both batch type and sequential type [24]-[28].

For the performance evaluation, we simulate four different scenarios. 1) All interferences are uncorrelated. 2) An interference signal is correlated with a desired signal by the multipath effect. 3) Interferences are time-varying as well as correlated. 4) Receiver moves under interference signal environments. In the simulation, we compare the proposed algorithm with the conventional Minimum Mean Square Error (MMSE), spatial smoothing MMSE for coherent interference cancellation and Radial Basis Function (RBF) network. From the simulation results, we confirm that the proposed algorithm can cancel interference in a small aperture array antenna without a reduction of the effective array elements (unlike the spatial smoothing method) and with less computational complexity.

2. Review of the Extreme Learning Machine (ELM) Algorithm

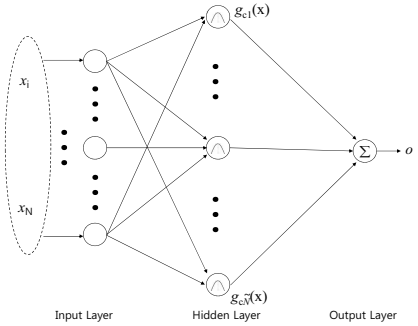

Fig. 1. ELM structure.

In this section, we review the ELM in [24] and [27]. Fig. 1 shows the typical structure of ELM. Given a series of arbitrary training samples ($\mathbf{x}(i)$,t(i)), $i = 1,2,\ldots,N$, where $\mathbf{x}(i) \in \mathrm{R}^p$ and $\mathrm{t}(i) \in \mathrm{R}^1$, the actual outputs of a single-hidden-layer feedforward network (SLFN) with activation function $\mathrm{g}_c(\mathrm{x})$ for these N training data is given by [24],[27]:

$$\sum_{k=1}^{\tilde{N}} \beta_k g_c(\mathbf{w}_k \cdot \mathbf{x}_i + b_k) = t_i, \quad i = 1,\cdots,N \tag{1}$$

where column vector $\mathbf{w}_k \in \mathrm{R}^p$ is the input weight vector connecting the input layer neurons to the k-th hidden neuron, $\beta_k \in \mathbf{R}^1$ is the output weight vector connecting the k-th hidden neuron and the output neuron, and $b_k \in \mathrm{R}^1$ is the bias of the k-th hidden neuron. $\mathbf{w}_k \cdot \mathbf{x}_i$ denotes the inner product of the column vectors $\mathbf{w}_k$ and $\mathbf{x}_i$. The above N equations can be written compactly as:

$$\mathbf{H}\beta = \mathbf{T}. \tag{2}$$

In practical applications the number $\tilde{N}$ of the hidden neurons is usually much less than the number N of training samples and **H**β=**T**, where:

$$\begin{aligned}&\mathbf{H}(\mathbf{w}_1,\cdots,\mathbf{w}_{\tilde{N}},\mathbf{x}_1,\cdots,\mathbf{x}_{\tilde{N}},b_1,\cdots,b_{\tilde{N}})\\ &= \begin{bmatrix} g_c(\mathbf{w}_1\cdot\mathbf{x}_1+b_1) & \cdots & g_c(\mathbf{w}_{\tilde{N}}\cdot\mathbf{x}_1+b_{\tilde{N}}) \\ \vdots & \ddots & \vdots \\ g_c(\mathbf{w}_1\cdot\mathbf{x}_N+b_1) & \cdots & g_c(\mathbf{w}_{\tilde{N}}\cdot\mathbf{x}_N+b_{\tilde{N}}) \end{bmatrix},\end{aligned} \tag{3}$$

$$\beta = \begin{bmatrix} \beta_1 \\ \vdots \\ \beta_{\tilde{N}} \end{bmatrix} \quad \text{and} \quad \mathbf{T} = \begin{bmatrix} t_1 \\ \vdots \\ t_N \end{bmatrix}. \tag{4}$$

Matrix **H** is called the hidden layer output matrix. For the fixed input weights $\mathbf{w}_i$ and the hidden layer biases b_i, we can obtain the least squares solution $\hat{\beta}$ of the linear system **H**β=**T** with the minimum norm of the output weights $\hat{\beta}$ (which usually tend to have a good generalization performance) from the results as analyzed by Huang *et al.* [24]. The resulting $\hat{\beta}$ is given by:

$$\hat{\beta} = \mathbf{H}^{+}\mathbf{T} \tag{5}$$

where $\mathbf{H}^{+}$ is the Moore–Penrose generalized inverse of matrix H. The three steps in the ELM algorithm can be summarized as follows:

ELM Algorithm: Given a training set N = $\{(\mathbf{x}(\mathrm{i})\ ,\ \mathrm{t(i)})|$ $\mathbf{x}(\mathrm{i}) \in \mathrm{R}^p$, $\mathrm{t(i)} \in \mathrm{R}^1$, i = 1, . . . ,N$\}$, activation function $\mathrm{g}_c(\mathrm{x})$, and hidden neuron number $\tilde{N}$:

1. Randomly choose the input weight $\mathbf{w}_k$ and the bias b_k, $k = 1,...,\tilde{N}$.
2. Calculate the hidden layer output matrix **H**.
3. Calculate the output weight $\hat{\beta}$ using (5).

The ELM algorithm is a batch type algorithm. Sequential ELM algorithms also have been developed [27]-[30]. Therefore, we can easily select a proper algorithm

type dependent on the application. For example, in the time-invariant cases, the batched type ELM algorithm was selected and a sequential ELM algorithm can be selected in time-varying cases. In addition, [27] described the distribution for random generation in step (1) as follows: Given any small positive value $\varepsilon > 0$ and activation function g(x): $R \to R$ which is infinitely differentiable in any interval, there exists $L \leq N$ such that for N arbitrary distinct input vectors $\{x_i | x_i \in R^n, i = 1, \cdots, L\}$, for any $\{(a_i, b_i)\}_{i=1}^{L}$ randomly generated according to any continuous probability distribution $\left\| \mathbf{H}_{N\times\tilde{N}} \beta_{L\times 1} - \mathbf{D}_{N\times 1} \right\| < \varepsilon$ with probability one [27].

3. Signal Model

Considering a uniform linear array of N sensors with element spacing of one half the carrier frequency wavelength, the beamforming snapshot x(n) consists of a desired signal from direction θ_s, q undesired (interference) signals from directions $\{\theta_1, \theta_2, \cdots, \theta_q\}$ and additive white noise, that is

$$\begin{aligned} x(n) &= s_s(n)a(\theta_s) + \sum_{k=1}^{q} s_k(n)a(\theta_k) + n(n) \\ &= x_s(n) + x_i(n) \end{aligned} \tag{6}$$

where $s_k(n) = p_k e^{j(\omega_0 n + \theta_k)}$ and $s_s(n) = p_s e^{j(\omega_0 n + \theta_0)}$ are the k-th random interference waveforms and the signal waveform respectively; in addition, the steering vectors a(θ) can be modeled as plane waves.

$$a(\theta) = [\exp(jl_1\xi), \exp(jl_2\xi), \cdots, \exp(jl_N\xi)]^T \tag{7}$$

where, $\xi = (2\pi/\lambda)\sin\theta$, λ is the wavelength, l_i is the coordinate of the i-th sensor, and T denotes the transpose. We can divide the snapshot into the desired signal $x_s(t)$ and the undesired interference signal $x_i(t)$. The complex adaptive beamformer output with the weight vector $\mathbf{w}(n)$at time n can then be expressed as

$$y(n) = \mathbf{w}(n)^H \mathbf{x}(n) \tag{8}$$

where $(\cdot)^H$stands for Hermitian transpose.

If the impinging signals are coherent (i.e., the relative phases are fixed) then we have

$$\begin{aligned} x(n) &= s_s(n)a(\theta_s) + \sum_{k=1}^{q} s_k(n)a(\theta_k) + n(n) \\ &= \left(a(\theta_s) + \sum_{k=1}^{q} \gamma_k a(\theta_k) \right) s_s(n) + n(n) \end{aligned} \tag{9}$$

where the $\{\gamma_i\}$ are the fixed complex constants, $\gamma_i = \left(p_i/p_s\right) e^{j(\theta_i - \theta_s)}$, $i = 1 \cdots q$.

4. ELM (Extreme Learning Machine) based Coherent Interference Canceller

We must first digest two conventional linear adaptive array algorithms before introducing the proposed algorithm. Section 4.1 summarizes the minimum mean square error (MMSE) beamformer that minimizes the mean square error between the beamformer output and a given desired response. Section 4.2 summarizes the spatial smoothing algorithm. This algorithm is a typical linear adaptive algorithm to cancel out coherent interferences. Section 4.3 describes the proposed algorithm. ELM was applied to the beamforming algorithm.

4.1 MMSE Beamforming

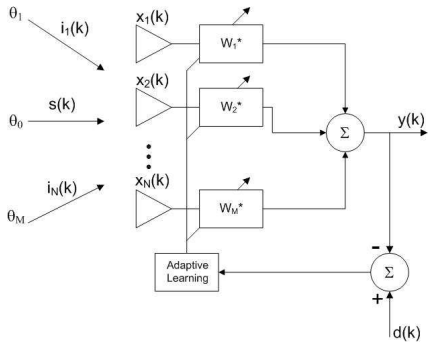

Fig. 2. MMSE beamforming.

The complex weights for each element of the array can be minimized for the Mean Square Error (MSE) of the difference between the array output and the reference signal. The obtained weights are not necessarily those that maximize the beam pattern in the direction of the desired user. This adaptive beamforming is an approximation of optimum beamforming.

The performance criteria minimizes the Mean Square Error between the received and the transmitted signals; therefore, the cost function to be minimized is given as [16],[31]

$$J = E\left(|d(n) - y(n)|^2 \right) \tag{10}$$

where E[.] denotes the ensemble average. Substituting for the output of the beamformer as $y(n) = \mathbf{w}^H \mathbf{x}(n)$ and taking of the gradient of the cost function and setting it to zero, we get:

$$\nabla J = -2\mathbf{r}_{xd} + 2\mathbf{R}_{xx}\mathbf{w} = 0 \tag{11}$$

where $\mathbf{R_{xx}} = E\left(\mathbf{x}(n)\mathbf{x}^H(n)\right)$ is the M $\times$ M correlation matrix of the input signal x(n). In adiition, $\mathbf{r}_{xd} = E\left(\mathbf{x}(n)d^*(n)\right)$ is the cross-correlation vector between the sensor inputs and the desired signal d(n). Solving (11) gives the expression for the optimum weights for MMSE as [16],[31]

$$\mathbf{w} = \mathbf{R}_{xx}^{-1}\mathbf{r}_{xd}. \tag{12}$$

4.2 Spatial Smoothing Method

The conventional MMSE in Section 4.1 fails in a coherent interference environment when the signals from undesired directions are strongly correlated. A spatial smoothing (averaging) technique may be applied to improve the covariance matrix estimate [17],[18]. For this technique, the original antenna array is subdivided into overlapping subarrays with a reduced aperture and the spatial covariance matrix estimate is obtained by averaging the spatial subarray covariance matrices.

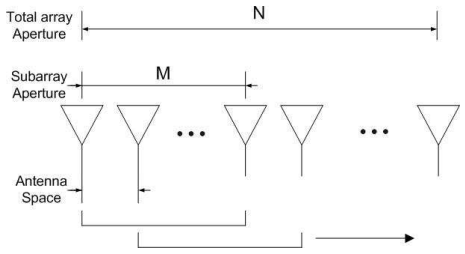

Fig. 3. Spatial smoothing for coherent environment.

Mathematically the spatial smoothing process can be represented as

$$\mathbf{R}_x = \frac{1}{N-M+1}\sum_{i=1}^{N-M+1}\mathbf{R}_x(n)_i \tag{13}$$

where $\mathbf{R}_x(n)_i = \mathbf{x}_i(n)\mathbf{x}_i(i)^H$ is the subarray spatial covariance matrix, M number of elements in a subarray and $\mathbf{x}_i(n) = [x_i(n), x_{i+1}(n), ..., x_{i+M-1}(n)]^T$ is the signal vector received by the i-th subarray.

$$\mathbf{r}_{xd} = \frac{1}{N-M+1}\sum_{i=1}^{N-M+1}\mathbf{r}_{xd}(n)_i, \tag{14}$$

where $\mathbf{r}_{xd}(n)_i = \mathbf{x}_i(n)d^*(n)$.

4.3 Proposed ELM based Beamforming

Fig. 4 shows that ELM can be applied to the interference canceller. The concept is quite similar to the MMSE beamforming in Fig. 2. In Section 2, we reviewed that training an ELM is only to find the weight parameter $\hat{\beta}$ since the input weights and the hidden layer bias were randomly chosen in the first step of learning. It satisfies

$$\left|\mathbf{H}\hat{\beta} - \mathbf{D}\right| = \min_{\beta}|\mathbf{H}\beta - \mathbf{D}| \tag{15}$$

where $|\cdot|$ is the Euclidean norm. $\mathbf{D} = [d(1), \cdots, d(N)]^T$, and $\mathbf{A}^T$ is the transposition of matrix $\mathbf{A}$. Equation (10) is equivalent to minimize the cost function as follows:

$$J = \sum_{n=1}^{N}(d(n) - y(n))^2 = \sum_{j=1}^{N}\left(d(j) - \sum_{i=1}^{\tilde{N}}\beta_i g(\mathbf{w}_i \cdot \mathbf{x}_j + b_i)\right)^2. \tag{16}$$

The above equation can be written in the vector form as

$$J = (\mathbf{H}\beta - \mathbf{D})^T(\mathbf{H}\beta - \mathbf{D}). \tag{17}$$

Section 2 showed that the least square estimate of β to minimize the cost function in (17) can be written as

$$\hat{\beta} = \left(\mathbf{H}^T\mathbf{H}\right)^{-1}\mathbf{H}^T\mathbf{D}. \tag{18}$$

As we mentioned in Section 2, the parameter $\hat{\beta}$ in (18) can also be derived sequentially using the sequential ELM algorithms in [27]-[30].

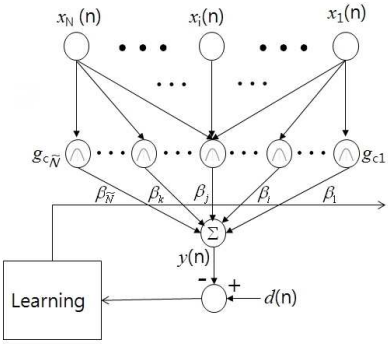

Fig. 4. Proposed ELM based interference canceller.

5. Simulation Results

In this section, computer simulations demonstrated the performance of the proposed beamformer. The received signals in all simulation examples were generated based on the model described in Section 2. We assume a uniform linear array with 4 elements with half-wavelength spacing. We used 8 hidden neurons and the activation function used in this simulation was a fully complex-valued activation function, the sech() response characteristic was similar to the Gaussian characteristics [32],[33]. The activation function used is provided in (19).

$$f_i(\mathbf{x}) = \text{sech}\left(\mathbf{v}_i^T(\mathbf{x} - \mathbf{c}_i)\right) \tag{19}$$

where $\mathbf{v}_i$, the complex-valued scaling factor of the i-th neuron and $\mathbf{c}_i$, the center of the i-th neuron. For the cancellation performance comparison, we compared MMSE, spatial smoothing based MMSE and RBF (Radial Basis Function) with the proposed algorithm. Each sub-array had 3 array elements in the spatial smoothing based MMSE.

In this simulation, we considered a data frame of 1 ms duration, structured with training period and payload period (see Fig. 5). The symbol rate is 1.28 Msymbol/sec. We assume the sampling rate is the same as the symbol rate. The training period consisted of 128 symbols. We set the training signal $\cos 0.4\pi n$, where 0.4π is normalized frequency as $2\pi f/f_s$ and f_s means sampling frequency. We set the payload symbols with randomly generated QPSK signals.

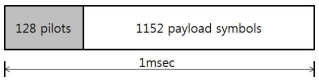

Fig. 5. Data frame structure in this simulation.

In 1 msec intervals, beamformer is trained for 0.1 msec (128 symbols). After training, the trained beamformer is used to receive the following payload symbols. The generated QPSK is $\pm 1 \pm j$. Fig. 6 shows the reference constellation diagram. We can evaluate the quality of the retrieved signal based on the constellation diagram in Fig. 6. All the simulations are carried out in the MATLAB 6.5 environment running on an ordinary PC with 3.2 GHz AMD CPU.

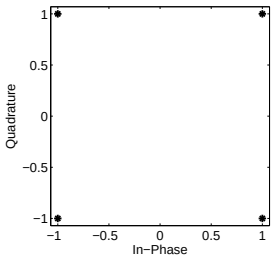

Fig. 6. Constellation of the generated QPSK signal.

5.1 Determine the Number of Hidden Neurons

For the activation function, the centers $\mathbf{c}_i$ are randomly selected from the range [-1 1]. It is usually used in ELM based research [25],[24],[26],[27]. It is reasonable in the receiving beamformer because the received signal exists in the limited range due to the preamplifier in the receiver. The complex-valued scaling factor is also selected for the uniform distribution. The following simulations that determine the number of hidden neurons selects the range. In addition, we should predetermine the number of hidden neurons by simulations because there is no analytical solution for the optimal number of hidden neurons in ELM [24].

For the simulation, we have a training signal $\cos 0.4\pi n$ arriving at 0° and one interfering signal which correlated to the training signal $0.9\cos(0.4\pi n + 0.005\pi)$ arriving at -60°. In this simulation, we set different ranges, such as 10, 1, 0.1 and 0.01, of the uniform distribution for the complex-valued scaling factor. Fig. 7 shows SINR improvement comparison with the different hidden number of neurons and the different range of the scaling factor: (a) case of range of the scaling factor 10 (b) case of range of the scaling factor 1 (c) case of range of the scaling factor 0.1 (d) case of range of the scaling factor 0.01.

We use the SINR improvement for the performance evaluation. The SINR improvement means the difference between the output SINR and the input SINR. Therefore, a larger SINR results in a superior interference cancellation. Fig. 7 shows the results of the SINR improvement depending on the different uniform distribution ranges for the scaling factor generation; in addition, Fig. 7 shows the confidence interval for each number of hidden neurons. The SINR improvement performance increases as the range of uniform distribution decreases; however, performance results of less than 0.1 are almost the same. In this simulation, we select 6 hidden numbers and generate the scaling factor in the uniform distribution, [-0.01, 0.01].

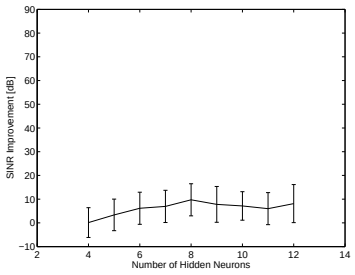

(a) Case of range of the scaling factor 10

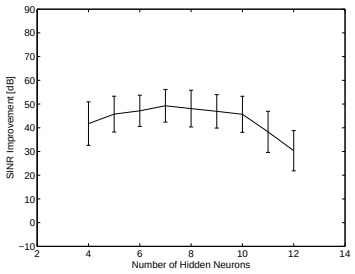

(b) Case of range of the scaling factor 1

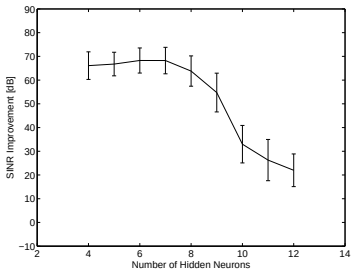

(c) Case of range of the scaling factor 0.1

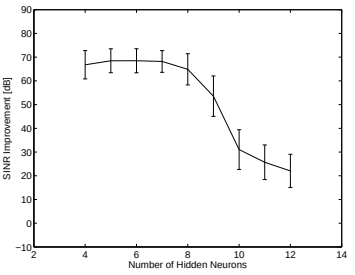

(d) Case of range of the scaling factor 0.01

Fig. 7. SINR improvement comparison with the different hidden number of neurons and the different range of the scaling factor.

5.2 Non Correlated Interference Case

In this case, we have a reference signal arriving at 0° and two interfering signals arriving at -60° and -30°. Each

signal has the same length with the reference signal. The interferences are generated by a white Gaussian noise generator for the non-correlated interference. All signal to interference ratios (SIRs) are set to 0 dB, respectively (see Fig. 8). Fig. 8 shows that all beamforming methods cancel out the interference successfully. The constellation results in Fig. 9 show that all methods retrieve symbols in the payload part successfully. In addition, we add another non-correlated interference arriving at 50°. The interference is also generated by a white Gaussian noise generator. The SIR sets to 0 dB. Fig. 10 shows the cancellation result. In Fig. 10, the spatial smoothing method fails in cancellation because the effective aperture size is reduced to 3 by smoothing so that 3 antenna elements can cancel up to 2 interferences. However, the proposed algorithm (as well as the conventional MMSE algorithm) still rejects the interference.

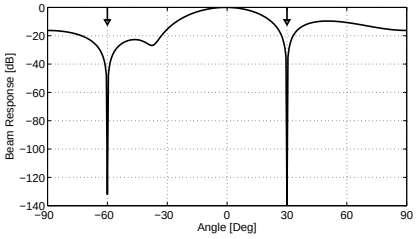

(a) MMSE method

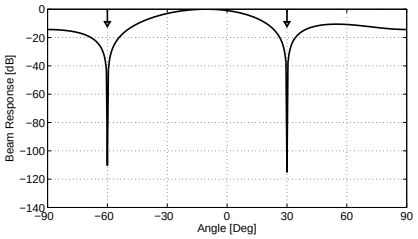

(b) Spatial smoothing method

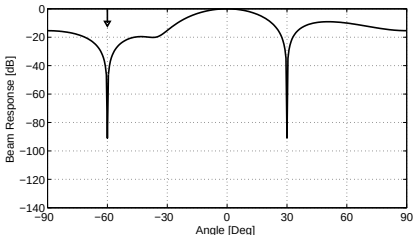

(c) RBF based method

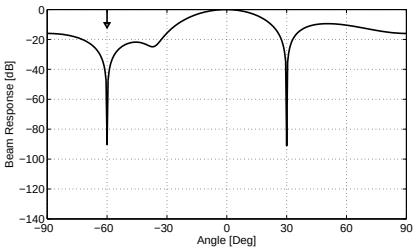

(d) Proposed ELM based method

Fig. 8. Interference canceling results for 2 non-correlated interferences case.

The constellation results in Fig. 11 also show that all methods (except for the spatial smoothing method) retrieve symbols in the payload part successfully. Fig. 8 and Fig. 10 show that RBF can cancel the interference effectively. RBF needs more computation complexity for training because RBF should train centers, scaling factors of activation functions and weighting coefficients between hidden neurons and output; however, the proposed ELM based algorithm trains only weighting coefficients between the hidden neurons and output. Tab. 1 and Tab. 2 summarize the SINR improvement results and the computation complexities for training. In order to compare the complexity of each algorithm, we use one of MATLAB commands, flops, to return the cumulative number of floating-point operations and the results are contained in the tables.

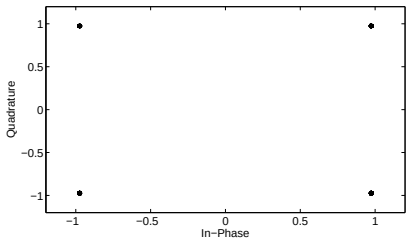

(a) MMSE method

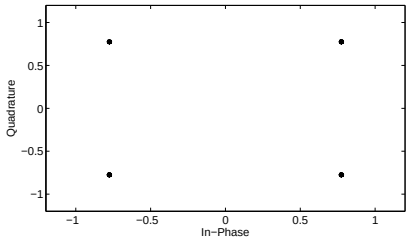

(b) Spatial smoothing method

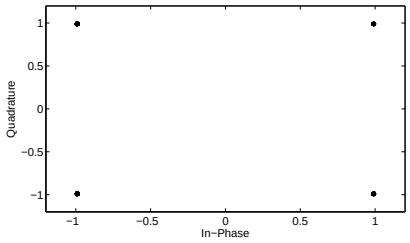

(c) RBF based method

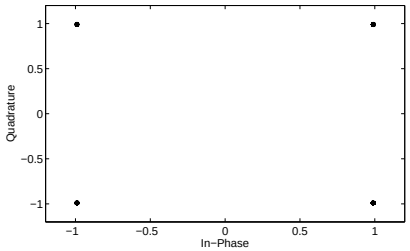

(d) Proposed ELM based method

Fig. 9. Constellation results for 2 non-correlated interferences case.

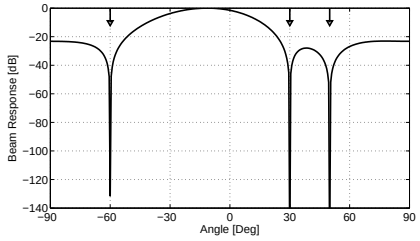

(a) MMSE method

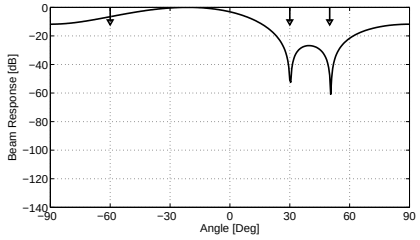

(b) Spatial smoothing method

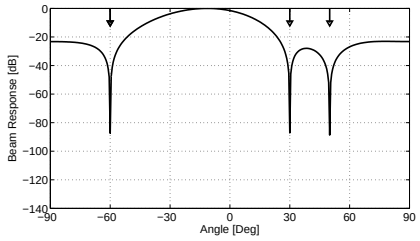

(c) RBF based method

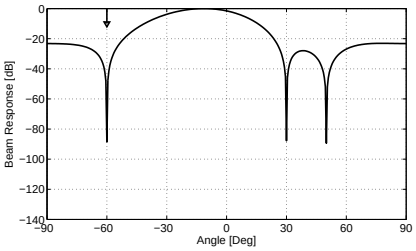

(d) Proposed ELM based method

Fig. 10. Interference canceling results for 3 non-correlated interferences case.

Algorithm	SINR improvement [dB]	Training Complexity [flops[1)]]
The proposed algorithm	104.9	347322.22
RBF	106.9	12737201.23
MMSE	135.2	12168.30
MMSE with spatial smoothing	110.9	16224.40
1) Flops has been measured in MATLAB using flops command.		

Tab. 1. SINR improvement results and computation complexity for 2 non-correlated interferences case.

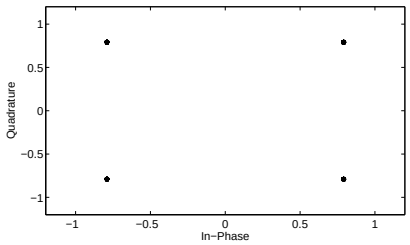

(a) MMSE method

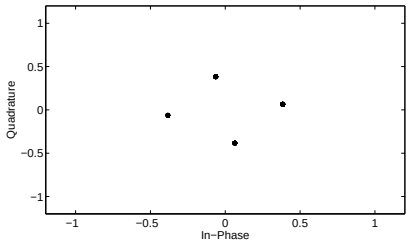

(b) Spatial smoothing method

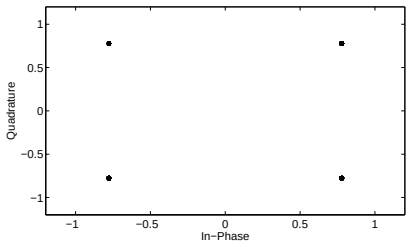

(c) RBF based method

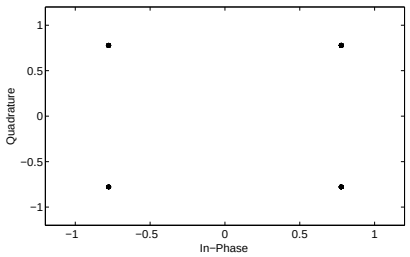

(d) Proposed ELM based method

Fig. 11. Constellation results for 3 non-correlated interferences case.

Algorithm	SINR improvement [dB]	Training Complexity [flops]
The proposed algorithm	104.1	348524.03
RBF	105.0	13026836.72
MMSE	135.3	8412.65
MMSE with spatial smoothing	NA	-
NA: The method fails to cancel interferences.		

Tab. 2. SINR improvement results and computation complexity for 3 non-correlated interferences case.

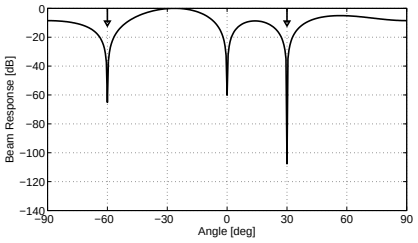

(a) MMSE method

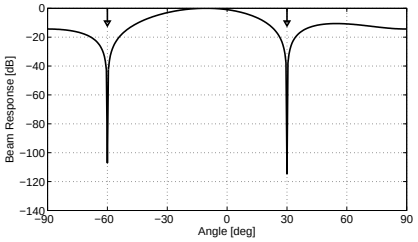

(b) Spatial smoothing method

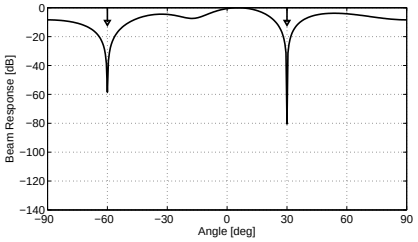

(c) RBF based method

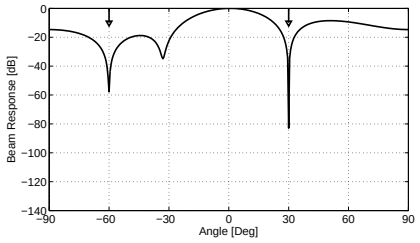

(d) Proposed ELM based method

Fig. 12. Interference canceling results for one correlated interference and one un-correlated interference case.

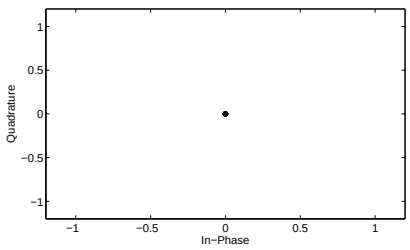

(a) MMSE method

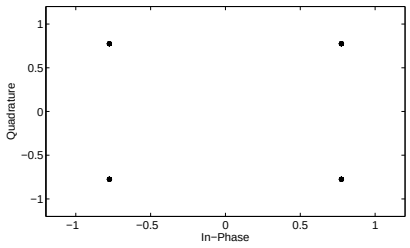

(b) Spatial smoothing method

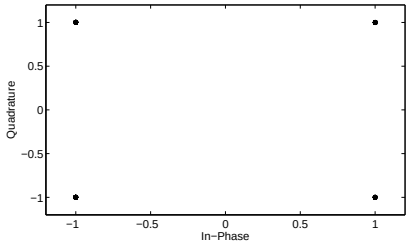

(c) RBF based method

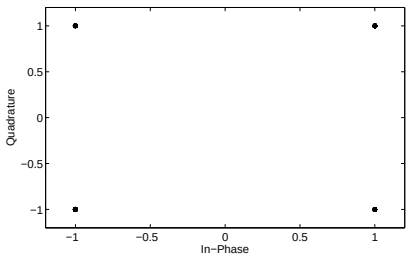

(d) Proposed ELM based method

Fig. 13. Constellation results for one correlated interference and one un-correlated interference case.

5.3 Multi-Path Training Signal Case

In this experiment, we simulated the multipath effect in the training signal. Through this experiment, we simulated the correlated interference effect. For this case, we have a reference signal arriving at 0° of which training part is $\cos(0.4\pi n)$and two interfering signals, one of which correlated with the training signal in the reference signal, $0.9\cos(0.4\pi n + 0.005\pi)$, arriving at -60°. The other interference is a non-correlated one. The arrival angle is 30° and its SIR is set to 0 dB. Fig. 12 shows that all beamforming methods except for MMSE method cancel out the interference successfully. The constellation results in Fig. 14 show that all methods except for the MMSE method retrieve symbols in the payload part successfully.

In addition, we add another non-correlated interference arriving at 50°. The interference is also generated by a white Gaussian noise generator. The SIR is set to 0 dB. Fig. 15 shows that only the proposed method cancels out the interference successfully. That means the proposed algorithm can utilize full array aperture unlike spatial smoothing method.

In addition, we add another non-correlated interference arriving at 50°. The interference is also generated by a white Gaussian noise generator. The SIR is set to 0 dB. Fig. 15 shows that only the proposed method and RBF cancel out the interference successfully. We can confirm this by the constellation results in Fig. 16, which also show that the proposed method and RBF cancel retrieve symbols in the payload part successfully. The results in RBF was expected in

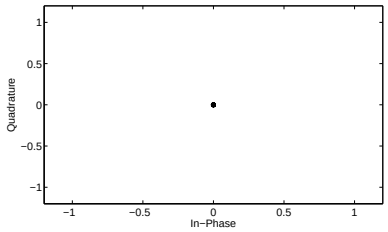

(a) MMSE method

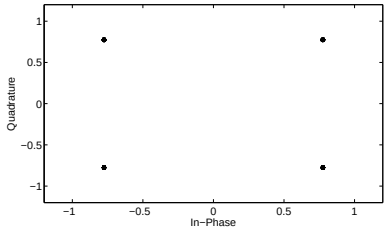

(b) Spatial smoothing method

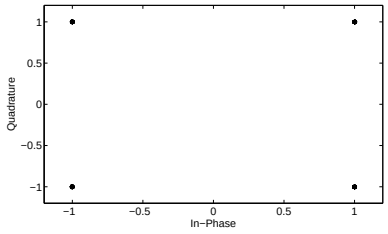

(c) RBF based method

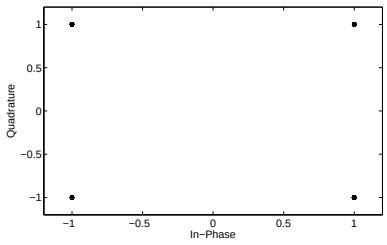

(d) Proposed ELM based method

Fig. 14. Constellation results for one correlated interference and one un-correlated interference case.

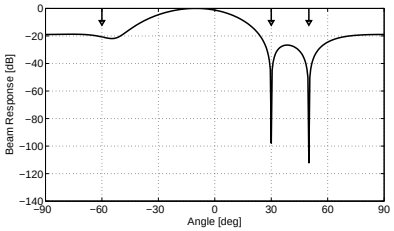

(a) MMSE method

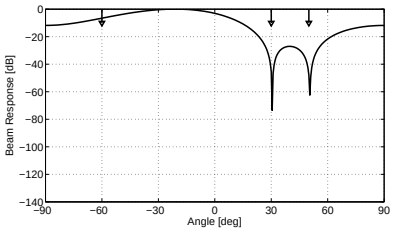

(b) Spatial smoothing method

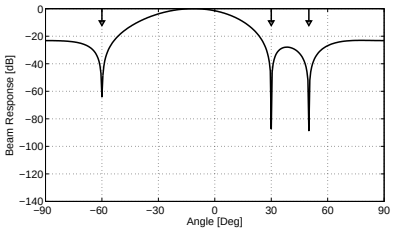

(c) RBF based method

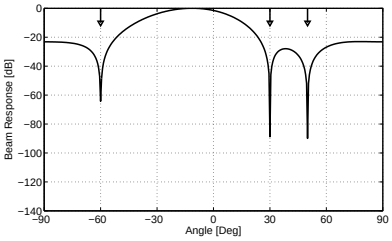

(d) Proposed ELM based method

Fig. 15. Interference canceling results for one correlated interference and two un-correlated interferences case.

Algorithm	SINR improvement [dB]	Training Complexity [flops]
The proposed algorithm	74.1	349725.84
RBF	74.5	12862189.16
MMSE	NA	-
MMSE with spatial smoothing	108.6	11567.39
NA: The method fails to cancel interferences.		

Tab. 3. SINR improvement results and computation complexity for one correlated interference and one un-correlated interference case.

Algorithm	SINR improvement [dB]	Training Complexity [flops]
The proposed algorithm	75.4	358438.94
RBF	75.5	12960286.65
MMSE	NA	-
MMSE with spatial smoothing	NA	-
NA: The method fails to cancel interferences.		

Tab. 4. SINR improvement results and computation complexity for one correlated interference and two un-correlated interferences case.

[19]; however, RBF requires more computation complexity in Tab. 3 and Tab. 4. Tab. 3 and Tab. 4 summarize the SINR improvement results and the required training complexity. The results in this section confirm that the proposed algorithm is the most suitable as a correlated interference canceller for a small aperture array antenna.

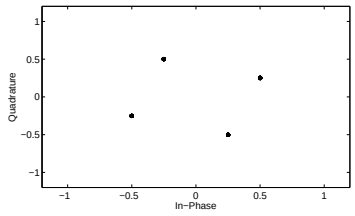

(a) MMSE method

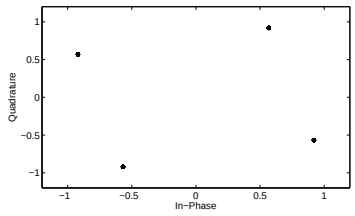

(b) Spatial smoothing method

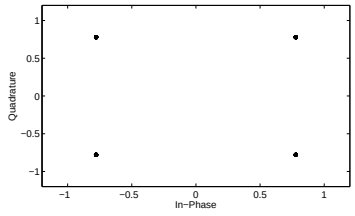

(c) RBF based method

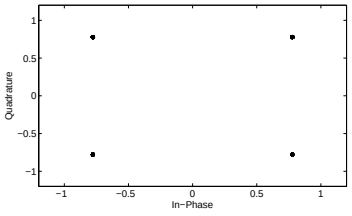

(d) Proposed ELM based method

Fig. 16. Constellation results for one correlated interference and two un-correlated interferences case.

5.4 Time-Varying Inferences Case

This experiment simulated the time-varying interference effect. We have a reference signal arriving at 0° and three interfering signals are non-correlated with the reference signal. In the first case, we consider three uncorrelated interferences: two fixed interferences arriving at -60° and 30° as well as a time-varying interference of which the arriving angle is 50° and then abruptly changes from 50° to 60° at 65^{th} time step. We set to update the array weight at every 32 time steps in order to handle the time-varying interferences. This update was similar to the conventional Sample Matrix Inversion (SMI) based adaptive beamformer [16]. Fig. 17 shows that all the algorithms except for the spatial smoothing algorithm cancel out the interference successfully. The reason why the spatial smoothing algorithm fails is that the effective element number is reduced from 4 to 3 by spatial smoothing. An array with 3 elements can resolve only two interferences.

In the second case, we make one interference arriving at -60° correlated with the reference signal as $0.9\cos(0.4\pi n + 0.005\pi)$. The other arriving angle scenario is identical to the first case. Fig. 18 shows that only the proposed method cancels out the interference successfully.

5.5 Moving Receiver Case

This experiment simulated the moving receiver case. In this case we assumed a receiver moving in 60 km/h (≈ 16.7 m/sec). The signal specifications for the reference and three interferences are identical to the experiment in Section 5.3; in addition, we set the positions of each signals as in Fig. 19. In the training period, we also update the array weight at every 32 time steps as in Section 5.3. After the training, the beamformer is fixed during the payload interval as in Fig. 5. In order to show the moving effect, we compared the SINR improvements at the payload start point with those at the payload end point. We can confirm that the moving effect can be handled by the time interval between the training and the next training. Table 5 summarizes the SINR improvement changes. Table 5 also shows that there is small change in SINR improvement even in the moving receiver case. This result comes from the data structure in Fig. 5, in which the training period is 1 msec. SINR improvement results for the moving receiver can change depending on the training period.

Algorithm	SINR improvement at the start of payload	SINR improvement at the end of payload
The proposed algorithm	60.55 dB	54.04 dB
RBF	60.83 dB	54.29 dB
MMSE	NA	NA
MMSE with spatial smoothing	NA	NA
NA: The method fails to cancel interferences.		

Tab. 5. SINR improvement variation results for moving receiver case.

6. Conclusion

This paper presented an ELM based coherent interference cancellation algorithm for a small aperture array antenna. We compared the proposed algorithm with a conventional MMSE algorithm, a spatial smoothing algorithm (famous for its coherent interference canceling ability) and RBF (typical nonlinear beamforming algorithm) for an SINR improvement comparison. The comparison showed a good advantage for the proposed algorithm. The advantage of the proposed method is that it uses a full aperture size in the antenna versus the spatial smoothing algorithm that uses only a reduced aperture size. The proposed algorithm maximizes the number of coherent interferences to cancel out, while the spatial smoothing algorithm reduces the number. In addition, the proposed algorithm requires substantially less computation complexity than RBF. This feature holds significant promise for a small aperture array antenna in a modern mobile communication device.

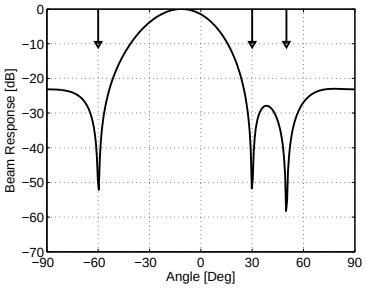

(a) MMSE method before angle change

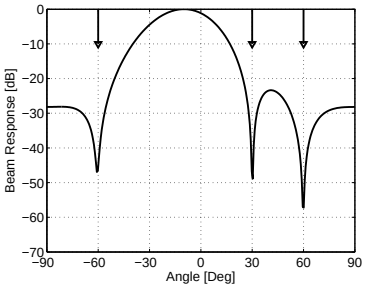

(b) MMSE method after angle change

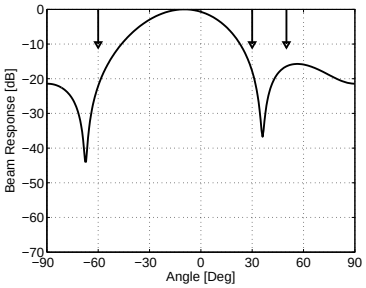

(c) Spatial smoothing method before angle change

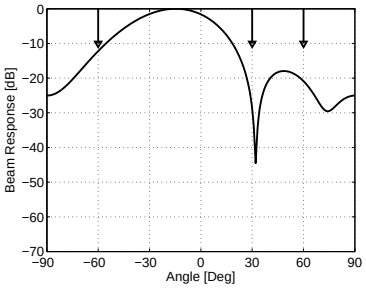

(d) Spatial smoothing method after angle change

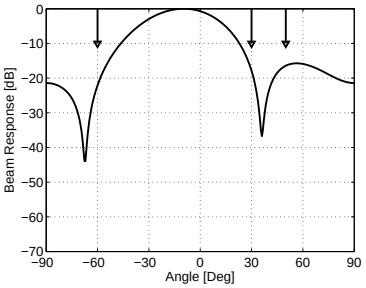

(e) RBF based method before angle change

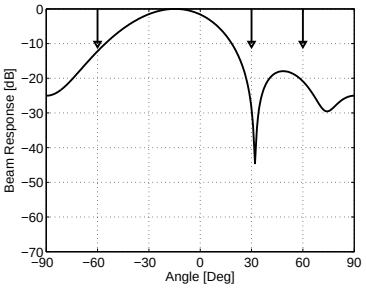

(f) RBF based method after angle change

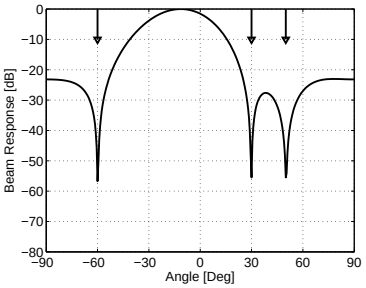

(g) Proposed ELM based method before angle change

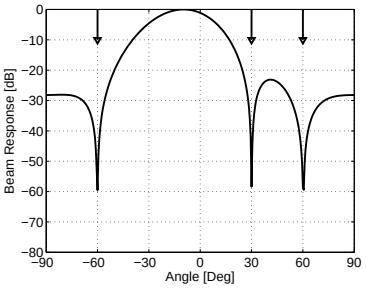

(h) Proposed ELM based method after angle change

Fig. 17. Time-varying interference canceling results for three non-correlated interferences case.

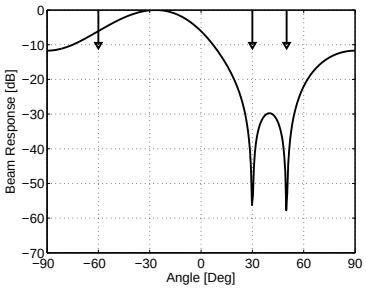

(a) MMSE method before angle change

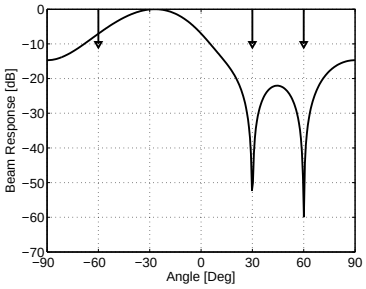

(b) MMSE method after angle change

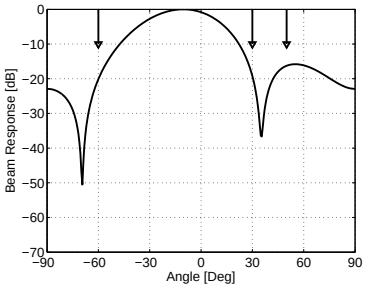

(c) Spatial smoothing method before angle change

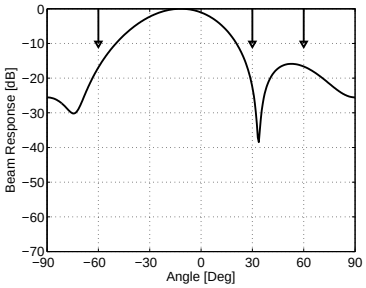

(d) Spatial smoothing method after angle change

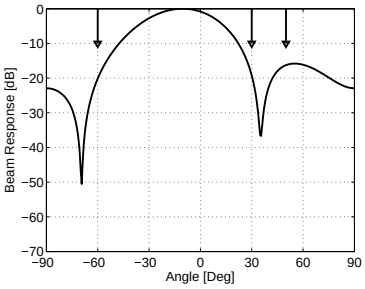

(e) RBF based method before angle change

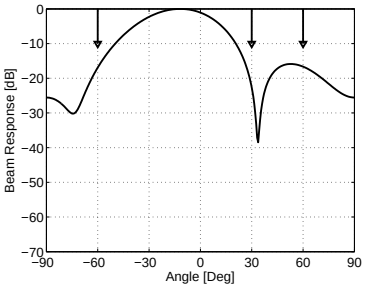

(f) RBF based method after angle change

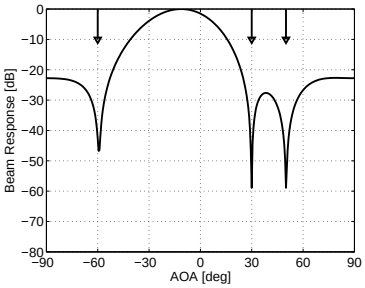

(g) Proposed ELM based method before angle change

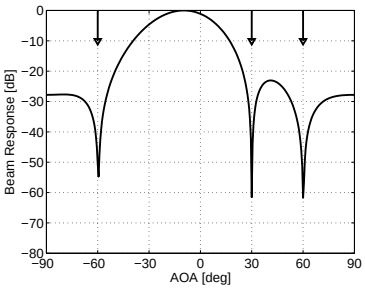

(h) Proposed ELM based method after angle change

Fig. 18. Time-varying interference canceling results for two un-correlated interferences and one correlated interference case.

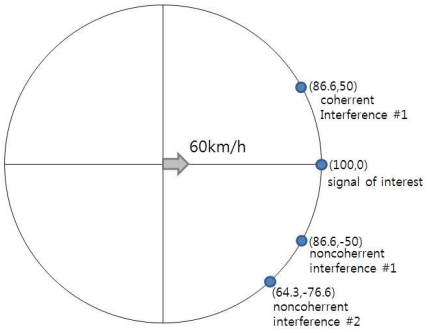

Fig. 19. Receiver and interferences scenario for moving receiver case.

Acknowledgements

This paper was supported by Agency for Defense Development (ADD) in Korean (UD130015DD).

References

[1] DIETRICH, J., STUTZMAN, W., KIM, B., DIETZE, K. Smart antennas in wireless communications: Base-station diversity and handset beamforming. *IEEE Antennas and Propagation Magazine*, 2000, vol. 42, no. 5, p. 142 - 151.

[2] JANG, Y. K., VILLASENOR, J. D. SINR improvement through reconfigurable antenna adaptation to handheld device orientation. In *Antennas and Propagation Society International Symposium (APSURSI)*. Toronto (Canada), 2010, p. 1 - 4.

[3] IDA, Y., AHN, C. J., KAMIO, T., FUJISAKA, H., HAEIWA, K. An interference cancellation scheme for TFI-OFDM in time-variant large delay spread channel. *Radioengineering*, 2009, vol. 18, no. 1, p. 75 - 82.

[4] KEJIK, P., HANUS, S. Enhanced receivers for interference cancellation in 3G systems. *Radioengineering*, 2009, vol. 18, no. 4, p. 477 - 484.

[5] JOSHI, G. G., DIETRICH, C. B. Jr., STUTZMAN, W. L. Adaptive beamforming measurements using four-element portable and mobile arrays. *IEEE Transactions on Antennas and Propagation*, 2005, vol. 53, no. 12, p. 4065 - 4072.

[6] SONG JOON-IL, LIM JUN-SEOK, CHOI NAKJIN, SUNG KOENG-MO Adaptive moving jammer cancellation algorithm for small aperture array. In *IEEE International Conference on Acoustics, Speech and Signal Processing (ICASSP)*. Orlando (USA), 2002, vol. 4, p. IV-4187.

[7] VUCETIC, B., YUAN, J. Space-time coding. *Handbook of Communication*. Chichester (England): Wiley, 2003.

[8] TAROKH, V., NAGUIB, A., SESHADRI, N., CALDERBANK, A. R. Space-time codes for high data rate wireless communications: Performance criteria in the presence of channel estimation errors, mobility, and multiple paths. *IEEE Transactions on Communications*, 1999, vol. 47, no. 2, p. 199 - 207.

[9] JUNTTI, M., VEHKAPERA, M., LEINONEN, J., ZEXIAN, V., TUJKOVIC, D., TSUMURA, S., HERA, S. MIMO MC-CDMA communications for future cellular systems. *IEEE Communications Magazine*, 2005, vol. 43, no. 2, p. 118 - 124.

[10] LI, J., LETAIEF, K. B., CAO, Z. Co-channel interference cancellation for space-time coded OFDM systems. *IEEE Transactions on Wireless Communications*, 2003, vol. 2, no. 1, p. 41 - 49.

[11] SULEESATHIRA, R. Co-channel interference cancellation for space-time coded OFDM systems using adaptive beamforming and null deepening. *Journal of Telecommunications*, 2010, vol. 1, no. 1, p. 6 - 13.

[12] OLADUNNI, F. J., STUART, J. W. Empirical performance evaluation of enhanced throughput schemes of IEEE802.11 technology in wireless area networks. *International Journal of Wireless and Mobile Networks (IJWMN)*, 2013, vol. 5, no. 4, p. 171 - 185.

[13] OLADUNNI, F. J., STUART, J. W. Investigation of beam forming effectiveness In IEEE802.11ac indoor wireless links. In *Proceedings of 3rd International Conference on Computer Science and Information Technology (CCSIT 2013)*. Bangalore (India), 2013, p. 27 - 35.

[14] BALTZIS, K. B. Spatial characterization of the uplink inter-cell interference in polygonal-shaped wireless networks. *Radioengineering*, 2013, vol. 22, no. 1, p. 363 - 370.

[15] GLEISSNER, F., HANUS S. Co-channel and adjacent channel interference measurement of UMTS and GSM/EDGE systems in 900 MHz radio band. *Radioengineering*, 2008, vol. 17, no. 3, p. 74 - 80.

[16] GROSS, F. *Smart Antenna for Wireless Communication*. New York (USA): McGraw-Hill, 2005.

[17] EVANS, J. E., JOHNSON, J. R., SUN, D. F. *Applications of Advanced Signal Processing Techniques to Angle of Arrival Estimation in ATC Navigation and Surveillance System,* rep. 582. Lexington (MA, USA): Lincoln Lab, 1982.

[18] REDDY, V. U., PAULRAJ, A., KAILIATH, T. Performance analysis of the optimum beamformer in the presence of correlated sources and its behavior under spatial smoothing. *IEEE Transactions on Acoustics, Speech and Signal Processing*, 1987, vol. 35, p. 927 - 936.

[19] LO, T., LEUNG, H., LITVA, J. Non linear beam forming. *Electronics Letters*, 1991, vol. 27, no. 4, p. 350 - 352.

[20] CESAR, C., GAUDES, J. V., SANTAMARIA, I. Robust array beamforming with sidelobe control using support vector machines. In *Fifth IEEE Workshop on Signal Processing Advances in Wireless Communications*. Lisbon (Portugal), 2004, p. 11 - 14.

[21] MOHAMMADZADEH, B., MAHLOOJIFA, A. Evaluation of the SVM-based adaptive beamformer in mismatch and no-mismatch scenarios. In *3rd International Sympostiuym on Communications, Control and Signal Processing (ISCCSP)*. St. Julians (Malta), 2008, p. 1127 - 1132.

[22] LIN, G., LI, Y., JIN, B. A new algorithm for robust adaptive beamforming. In *International Conference on Computer, Mechatronics, Control and Electronic Engineering (CMCE)*. Changchun (China), 2010, p. 104 - 107.

[23] WANG, L., JIN, G., LI, Z., XU, H. A nonlinear adaptive beamforming algorithm based on least squares support vector regression. *Sensors*, 2012, vol. 12, p. 12424 - 12436.

[24] HUANG, G. B. , WANG, D. H., LAN, Y. Extreme learning machines: A survey. *International Journal of Machine Leaning and Cybernetics*, 2011, vol. 2, no. 2, p. 107 - 122.

[25] HUANG, G. B. , ZHU, Q. Y. , SIEW, C. K. Extreme learning machine: Theory and applications. *Neurocomputing*, 2006, vol. 70, no. 12, p. 1 - 3.

[26] HUANG, G. B., ZHU, Q. Y., SIEW, C. K. Extreme learning machine: A new learning scheme of feedforward neural networks. In *Proceedings of International Joint Conference on Neural Networks*. Budapest (Hungary), 2004, p. 25 - 29.

[27] LIANG, N.-Y., HUANG, G. B., SARATCHANDRAN, P., SUNDARARAJAN, N. A fast and accurate online sequential learning algorithm for feedforward networks. *IEEE Transactions on Neural Networks*, 2006, vol. 17, no. 6, p. 1411 - 1423.

[28] LIM, J. S., JEON, J., LEE, S. Recursive complex extreme learning machine with widely linear processing for nonlinear channel equalizer. *Lecture Notes in Computer Science*, 2006, vol. 3973, p. 128 - 134.

[29] LIM, J. S. Partitioned online sequential extreme learning machine for large ordered system modeling. *Neurocomputing*, 2013, vol. 102, no. 11, p. 59 - 64.

[30] LIM, J. S., LEE, S. J., PANG, H. S. Low complexity adaptive forgetting factor for online sequential extreme learning machine (OS-ELM) for application to nonstationary system estimations. *Neural Computing and Applications*, 2013, vol. 22, no. 3, p. 569 - 576.

[31] HAYKIN S. *Adaptive Filter Theory*. 4th Fourth edition. New Jersey (USA): Prentice Hall, 2002.

[32] SAVITHA, R., VIGNESWARAN, S., SURESH, S., SUNDARARAJAN, N. Adaptive beamforming using complex-valued radial basis function neural networks. In *IEEE Region 10 Conference TENCON*. Singapore, 2009, p. 1 - 6.

[33] SAVITHA, R., SURESH, S., SUNDARARAJAN, N., KIM, H. J. A fully complex-valued radial basis function classifier for real-valued classification problems. *Neurocomputing*, 2012, vol. 78, no. 1, p. 104 - 110.

About Authors ...

Junseok LIM was born in Seoul, Korea. He received the B.E., the M.S. and Ph.D. degrees from Seoul National University, Korea, in 1986, 1988 and 1996 respectively. He worked as a Research Engineer for Agency for Defense Development in Korea from 1988 to 1993. From 1996 to 1997, he was with LG Electronics Company as a Senior Research Engineer. Since 1998, he has been with Sejong University in Seoul, Korea as a Professor. His research interests are acoustic signal processing and adaptive signal processing.

Heesuk PANG received the B.E., M.E., and Ph.D. degrees from Seoul National University in 1994, 1996, and 2001, respectively. From 2001 to 2008, he worked for LG electronics as a chief research engineer. Since 2008, he is an associate professor at the department of electronics engineering, Sejong University. His research interests include audio signal processing and audio coding.

Wooyoung HONG received a B.Sc. degree from the Republic of Korea Naval Academy in 1982 and a M.Sc. degree from Yonsei University, Seoul, Korea, in 1985 both in Electrical Engineering. He earned the Ph.D. in Electrical Engineering from the University of Minnesota in 1987. In 2008, he also completed the National Defense and Security Program at the Korea National Defense University, Seoul, Korea. He had been a faculty member of the Republic of Korea Navy since 1985, before leaving the Navy as a Captain in February 2013. From 1995 to 1997, he worked as a joint researcher with the Agency for Defense Development, Korea. From 1997 to 2000, he was an exchange professor at the Electrical Engineering Department of the U.S. Naval Academy in Annapolis, MD. Since 2013, he has been with Sejong University in Seoul, Korea as a Professor. His research interests are underwater acoustic signal processing including sonar signal processing, adaptive signal processing and naval tactics.